Space-Charge Effects on Multipactor on a Dielectric

Agust Valfells, John P. Verboncoeur, and Y. Y. Lau, *Member, IEEE*

***Abstract*—This paper analyzes the effects of space charge shielding on the steady state of multipactor discharge on a dielectric. Analytic methods are used to obtain an exact function for the potential in the discharge, assuming a Maxwellian distribution of emitted electrons. An equation for the amount of power deposited on the dielectric by the multipactoring electrons, for a given saturation level, is given. A simple method for obtaining the saturation level, for a given material, is obtained.**

***Index Terms*—Breakdown, multipactor, window failure.**

I. Introduction

MULTIPACTOR discharge on a dielectric is a secondary electron avalanche along the surface of a dielectric, driven by an RF wave. This phenomenon is commonplace and can be highly detrimental in high-power microwave devices. The secondary avalanche may deposit energy to the window to cause failure [1]–[9], or it may lead to flashover if plasma is formed along the surface, via desorption and subsequent ionization, of gas from the dielectric [8].

Earlier studies [6] of multipactor discharge on dielectric have focused on a kinematic theory for the conditions for multipactor initiation, as well as a dynamic theory of evolution of the discharge and its saturation mechanism [7]. The kinematic theory has led to the construction of generalized susceptibility diagrams, including the effects of external and RF magnetic fields, and of an oblique RF field on the dielectric [10]. The dynamic theory indicates that surface charging of the dielectric, rather than loading of the RF, provides the saturation mechanism, and that the power deposited on the dielectric, by the discharge, is on the order of 1% of the incident RF power.

The theories described above did not take into account the space charge effects of the electrons in the discharge. It was assumed that the multipactoring electrons are pulled back to the surface only by the positive charge that is left behind on the dielectric surface. The space charge effects are thus ignored. This is not a serious limitation in the case of the kinematic theory, in which we are mostly interested in the conditions leading up to multipactor discharge, and we may, therefore, ignore the space charge effects. Recently, Neuber *et al.* noted that the effects of space charge can significantly alter the impact energy of the multipactoring electrons [9]. Although not explicitly stated, their model assumed that the multipactoring electrons have a monoenergetic emission velocity. Their model also yielded the peculiar result that a 10% increase in emission energy can lead to a two order-of-magnitude increase in the impact energy. The apparent reason for this increase is that the monoenergetic beam assumption used to calculate the field profile leads to a sharp spatial cutoff in the restoring field. This process leads to something akin to an "escape velocity," whereby electrons emitted above that velocity (e.g., by 10%) are very weakly affected by the restoring field. It results in a long flight time and the opportunity to gain a large amount of energy.

In this paper, we focus on how the space charge affects the steady state. We assumed a Maxwellian distribution in the velocity of the emitted electrons. The potential distribution and density profiles for this one-dimensional (1-D) problem have been solved exactly. These analytic results have also been compared with those obtained from the particle simulation code XPDP1 [11]. The combined analytic theory and PIC-simulation allow us to examine the effects of the flux density of secondary electrons, of the distribution of emitted secondary electrons, and of the frequency and field strength of the RF driving the discharge. We will include a sample calculation of the energy spectrum of the electrons incident on the dielectric for typical parameters and, thus, compare the power deposited to the dielectric with the estimate from the simple dynamic theory (which ignores space charge effects). We will also discuss, briefly, some other effects, such as RF magnetic field, and finite geometry.

Section II describes the physical model used in our simulation. In Section III, we give a brief analysis of the problem. Section IV includes the most important results, and a few concluding remarks are made in Section V.

II. Model

To simulate the multipactor discharge at a given time, we use a 1-D, planar model. A schematic diagram is shown in Fig. 1. Electrons are injected from the left plate with a current density J_0, and a Maxwellian distribution with thermal velocity v_t. We concentrate on normally emitted current, even though some of our analysis allows for nonnormal emission of particles. An infinitesimal capacitor in series with the emitting plate, the "cathode," is used to replicate the dielectric behavior, whereby the injected current sets up an electric field, which pulls the electrons back to the emitting plate. A small number of electrons manage to traverse the gap, of length L, which leads to nonperfect shielding of the electric field across the gap. This is not unreasonable. As in a real device, some of the electrons emitted from the dielectric escape to the surrounding structure.

Manuscript received October 13, 1999; revised February 4, 2000. This work was supported by the Department of Energy, by the Multidisciplinary University Research Initiative (MURI) managed by the Air Force Office of Scientific Research and subcontracted through Texas Tech University and the University of California at Davis, under Contracts F49620-95-1-0333 and F49620-95-1-0253, and by the Northrop Grumman Industrial Associated Program.

A. Valfells and Y. Y. Lau are with the Department of Nuclear Engineering and Radiological Sciences, The University of Michigan, Ann Arbor, MI 48109-2104 USA (e-mail: yylau@umich.edu).

J. P. Verboncoeur is with the Department of Electrical Engineering and Computer Science, University of California, Berkeley, CA 94720 USA.

Publisher Item Identifier S 0093-3813(00)05363-7.

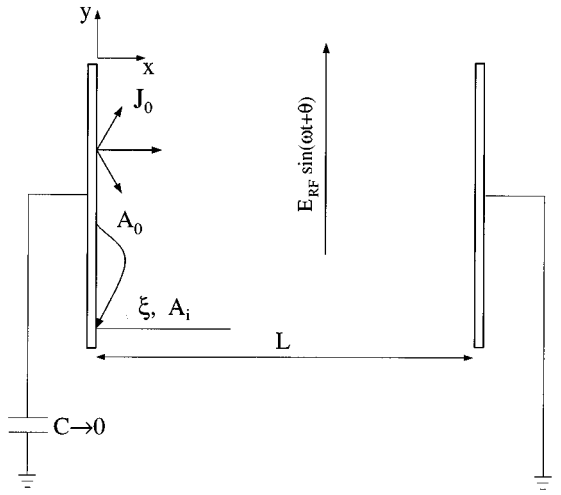

Fig. 1. Model used for analysis and numerical simulation of multipactor discharge. The emission energy is A_0, and the impact energy is A_i.

The emitted electrons are accelerated by an RF electric field, parallel to the cathode. Those electrons that do not traverse the diode then hit the cathode with an impact energy, A_i, and angle ξ. It should be noted that we make an electrostatic assumption; i.e., no spatial variation occurs in the RF fields. This assumption is valid up to the limit that the transverse excursion length is less than one-quarter of the RF wavelength.

To calculate the secondary electron emission caused by the flux of incident electrons, we use Vaughan's secondary emission model, which describes the secondary emission coefficient δ as a function of the impact energy A_i and impact angle ξ of the primary electron [12], [13].

$$\begin{aligned}
\delta(A_i, \xi) &= \delta_{\max}(\xi) \cdot \left\{ \frac{A_i}{A_{\max}(\xi)} \exp\left(1 - \frac{A_i}{A_{\max}(\xi)}\right) \right\}^{k(A_i)} \\
A_{\max}(\xi) &= A_{\max 0} \cdot \left(1 + \frac{k_s \xi^2}{\pi}\right) \\
\delta_{\max}(\xi) &= \delta_{\max 0} \cdot \left(1 + \frac{k_s \xi^2}{2\pi}\right) \\
k &= 0.435 - \frac{0.27}{\pi} \tan^{-1}\left(\pi \ln\left(\frac{A_i}{A_{\max}(\xi)}\right)\right). \qquad (1)
\end{aligned}$$

In the above formulas, $A_{\max 0}$ is the energy at which the secondary emission curve, for normally incident electrons, peaks (we use $A_{\max 0} = 420$ eV), $\delta_{\max 0}$ is the value of the secondary emission coefficient at that peak (we use $\delta_{\max 0} = 3$), and k_s is a parameter describing the surface roughness (we use $k_s = 1$, which is typical for a dull surface). In the analytic theory, we shall consider a steady-state problem with a constant emission current density, J_0. The consistent value of J_0 is taken to be the one that produces an average secondary yield, $\langle \delta \rangle = 1$.

The PIC code used, XPDP1 [11], has one spatial dimension of variation, and includes all three velocity components. We use an anode–cathode gap spacing, $L = 0.2$ m, and a time step, $\Delta t = 10^{-10}$ s. The grid is uniform with $N = 500$ cells. The number of electrons per macroparticle is 10^8. The code is nonrelativistic.

For the XPDP1 simulations, we use the following set of *standard parameters*:

$$\begin{aligned}
J_0 &= 10 \text{ A/m}^2 \\
v_t &= 6 \times 10^5 \text{ m/s} \\
E_{\mathrm{RF}} &= 16 \text{ kV/m} \\
f &= 0.1 \text{ GHz}.
\end{aligned}$$

These values are used in all runs of XPDP1, except for the parameter that is being varied at the time. The choice of the standard parameters is determined by two things: The average impact energy should be of the same scale as a typical value of the first crossover energy for a dielectric and by computational practicality. This rule limits us to the parameters above. The analytic solution is valid for general parameters.

III. Analysis

As multipactor discharge is believed to lead to vacuum window failure, it is of great interest to calculate the energy spectrum and the flux of the electrons incident on the dielectric to assess the power density of the impinging electrons. We will now derive some general relations for the average energy deposited on the dielectric, which are valid regardless of the characteristics of the injected current.

First, we wish to look at how much energy a primary electron may gain during its time of flight. Disregarding the RF magnetic field, the force equation for the direction along the electrode is (Fig. 1)

$$\ddot{y} = -\frac{eE_{\mathrm{RF}}}{m} \sin(\omega t + \theta). \qquad (2)$$

The energy gain from the RF electric field by the primary electrons, during one bounce, is

$$\Delta A_y = \tfrac{1}{2} m(\dot{y}^2(\tau) - v_{0y}^2) \qquad (3)$$

where τ is the time of flight of the electrons and v_{0y} is their initial velocity in the y-direction. This may be rewritten, after solving (2), as

$$\begin{aligned}
\Delta A_y = &\frac{v_{0y} e E_{\mathrm{RF}}}{\omega} \{\cos(\omega\tau + \theta) - \cos\theta\} \\
&+ \frac{e^2 E_{\mathrm{RF}}^2}{2m\omega^2} \{\cos(\omega\tau + \theta) - \cos\theta\}^2. \qquad (4)
\end{aligned}$$

Now, we can use this result to obtain the maximum energy that the RF field can impart to an electron in flight. It is clear from (4) that the imparted energy is at most

$$\Delta A_{y\max} = \frac{2|v_{0y}| e E_{\mathrm{RF}}}{\omega} + \frac{2e^2 E_{\mathrm{RF}}^2}{m\omega^2}. \qquad (5)$$

In the case $(m/e)|v_{0y}| \ll E_{\mathrm{RF}}/\omega$, we may neglect the first term on the right-hand side of (5) and expect to see a sharp dropoff in the energy spectrum at a value of

$$A_c = 8910 \left(\frac{E_{\mathrm{RF}}[\mathrm{MV/m}]}{f[\mathrm{GHz}]}\right)^2 [\mathrm{eV}]. \qquad (6)$$

To find the average impact energy, we may begin by averaging (4) over the emission phase, θ, which is assumed to have a uniform distribution from 0 to 2π. This eliminates the first term of the right-hand side of (4), and the average becomes

$$\langle \Delta A_y \rangle_\theta = \frac{e^2 E_{\mathrm{RF}}^2}{2m\omega^2} (1 - \cos \omega\tau). \tag{7}$$

To obtain the average impact energy $\langle A_i \rangle$, we average (7) over the flight time τ and add to it the average emission energy

$$\langle A_i \rangle = \langle A_0 \rangle + \int_0^\infty \frac{e^2 E_{\mathrm{RF}}^2}{2m\omega^2} (1 - \cos \omega\tau) g(\tau)\, d\tau \tag{8}$$

where $g(\tau)$ is the distribution function of the possible flight times and $\langle A_0 \rangle$ is the average emission energy.

Equations (4)–(8) are valid for any distribution of the emitted electrons. It is possible in some cases to obtain the flight time as an explicit function of the emission velocity, and a few other parameters characterizing the emission, such as the injection current density and thermal velocity, for example. This will be done later for a Maxwellian distribution of injected electrons.

For a general distribution $f(v_0)$ of the injected electrons, we may use energy conservation and the flux continuity of the electrons as a basis for determining the density profile

$$n(x) = \int_{\sqrt{(-2e\phi(x)/m)}}^\infty \frac{v_0 f(v_0)\, dv_0}{\sqrt{v_0^2 + \dfrac{2e\phi(x)}{m}}}. \tag{9}$$

Here, we make use of the fact that $dn_0 = f(v_0)\, dv_0$, the 1-D current conservation relation $en(x)v(x) = en_0\langle v_0 \rangle = J_0$, and the conservation of energy relation $v^2(x) = v_0^2 + 2e\phi(x)m^{-1}$. In some cases, at least, the integral on the right-hand side of (9) may be solved to yield a differential equation for the potential $\phi(x)$. In the case of a Maxwellian distribution of the injected electrons, it is possible to obtain explicit equations for the potential and the time of flight. With

$$f(v_0) = \frac{2n_0}{\sqrt{\pi} v_t} \exp\left(\frac{-v_0^2}{v_t^2}\right) \tag{10}$$

(9) can be evaluated explicitly and Poisson's equation becomes

$$\frac{\partial^2 \phi(x)}{\partial x^2} = \frac{en_0}{\varepsilon_0} \exp\left(\frac{e\phi(x)}{kT}\right) \tag{11}$$

where $kT = mv_t^2/2$. Equation (11) has the solution (which may be verified by direct substitution)

$$\phi(x) = \frac{-E_0 v_t}{\omega_p} \ln\left(1 + \frac{\omega_p}{v_t} x\right) \tag{12}$$

where the surface electric field E_0 is given by

$$E_0 = \sqrt{\frac{2kTn_0}{\varepsilon_0}} \tag{13}$$

and the plasma frequency at the surface ω_p is given by

$$\omega_p = \sqrt{\frac{n_0 e^2}{\varepsilon_0 m}}. \tag{14}$$

Note that (12) gives

$$n(x) = n_0 \left(1 + \frac{\omega_p}{v_t} x\right)^{-2} \tag{15}$$

and that $E_0 = \sigma_0/\varepsilon_0$, where $\sigma_0 = e\int_0^\infty n(x)\, dx$. Note that the upper limit of integration assumes a semiinfinite system. For the bounded system as in the XPDP1 simulations, and the model depicted in Fig. 1, the same result is obtained by adding the "anode" wall charge.

From energy conservation, we obtain the following expressions describing the upward motion of an electron emitted with velocity v_0 in a potential described by (12):

$$\frac{\partial x}{\partial t} = \sqrt{v_0^2 - 2v_t^2 \ln\left(1 + \frac{\omega_p}{v_t} x\right)} \tag{16}$$

and via direct integration

$$\sqrt{\frac{\pi}{2}} \frac{\exp\left(\dfrac{v_0^2}{2v_t^2}\right)}{\omega_p} \cdot \left\{ \operatorname{erf}\left(\sqrt{\frac{v_0^2}{2v_t^2}}\right) - \operatorname{erf}\left(\sqrt{\frac{v_0^2}{2v_t^2} - \ln\left(1 + \frac{\omega_p}{v_t} x\right)}\right) \right\} = t. \tag{17}$$

The height of the trajectory $x_{\max}$ of an electron emitted with velocity v_0 is found by setting the right-hand side of (16) equal to zero

$$x_{\max} = \frac{v_t}{\omega_p} \left\{ \exp\left(\frac{v_0^2}{2v_t^2}\right) - 1 \right\}. \tag{18}$$

Realizing that an electron reaches the pinnacle of its trajectory after half the flight time, we obtain from (17) the following expression for the time of flight τ:

$$\tau = \sqrt{2\pi} \frac{\exp\left(\dfrac{v_0^2}{2v_t^2}\right) \operatorname{erf}\left(\sqrt{\dfrac{v_0^2}{2v_t^2}}\right)}{\omega_p}. \tag{19}$$

Having obtained $\tau(v_0)$, some scaling laws become apparent. First of all, let us look at the average impact energy

$$\langle A_i \rangle = \langle A_0 \rangle + \frac{1}{n_0} \int_0^\infty \frac{e^2 E_{\mathrm{RF}}^2}{2m\omega^2} (1 - \cos\{\omega\tau(v_0)\}) f(v_0)\, dv_0 \tag{20}$$

which with the substitution $y \equiv v_0^2/v_t^2$ becomes

$$\langle A_i \rangle = \langle A_0 \rangle + \frac{e^2 E_{\mathrm{RF}}^2}{2m\omega^2} G\left(\frac{\omega}{\omega_p}\right) \tag{21}$$

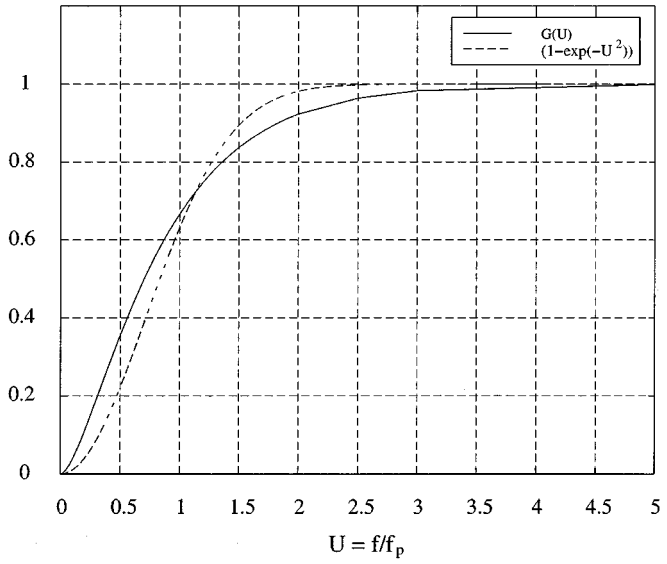

Fig. 2. Comparison of averaging functions for shielded, $G(U)$, and nonshielded, $1-\exp(-U^2)$, multipactor.

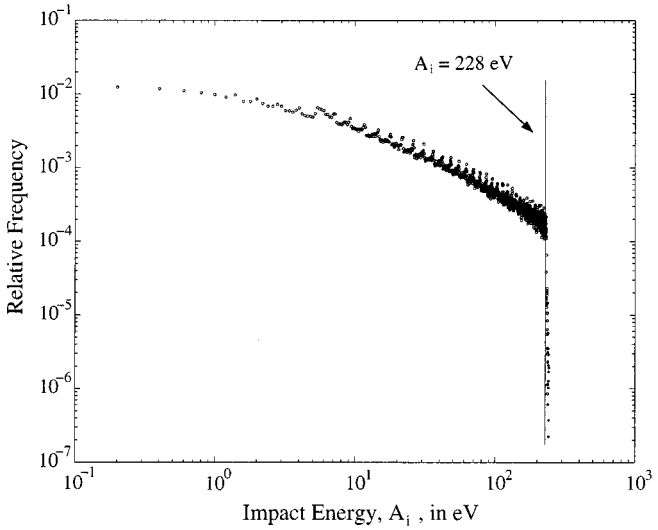

Fig. 3. Impact energy spectrum from XPDP1 using the standard parameters (see Section II). The vertical line denotes the value of the impact energy, A_i, equal to the drop-off energy, A_c, as given by (6).

where we define

$$G\left(\frac{\omega}{\omega_p}\right) \equiv 1 - \frac{2\sqrt{2}}{\sqrt{\pi}} \int_0^\infty \cos\left(\sqrt{2\pi}\,\frac{\omega\,\exp(y^2)\,\mathrm{erf}(y)}{\omega_p}\right) \cdot \exp(-2y^2)\,dy. \tag{22}$$

The function defined in (22), which may be called an *averaging function*, describes all of the effects of the injection current. Interestingly, it is solely dependent on the ratio ω/ω_p, and completely independent of the temperature of the injected current (the temperature manifests in the average impact energy only via the average emission energy, which may usually be neglected). The averaging function is useful when we later calculate the power deposited on the dielectric. It is shown in Fig. 2.

For the Maxwellian distribution, the injection current density J_0 is given by

$$J_0 = \frac{\sqrt{\pi} n_0 e v_t}{2}. \tag{23}$$

The power P, per unit area, deposited on the dielectric by the incident electrons is

$$P = \langle A_i \rangle J_0/e = \frac{\sqrt{\pi}}{4}\left(2\langle A_0\rangle \frac{m\varepsilon_0}{e^2}\,\omega_p^2 v_t + \varepsilon_0 v_t E_{\mathrm{RF}}^2 \left(\frac{\omega_p}{\omega}\right)^2 G\left(\frac{\omega}{\omega_p}\right)\right). \tag{24}$$

It is of some interest to compare these results to those obtained when space charge effects are ignored. In the latter case, an emitted electron is subject only to the surface electric field E_0 [of (13)]. The flight time then becomes

$$\tau_{NC} = \frac{2v_0}{\omega_p v_t} \tag{25}$$

and the average incident energy is

$$\langle A_{iNC}\rangle = \langle A_0\rangle + \frac{e^2 E_{\mathrm{RF}}^2}{2m\omega^2}\left(1 - \exp\left(-\frac{\omega^2}{\omega_p^2}\right)\right) \tag{26}$$

whereas the power deposited per unit area is given by

$$P_{NC} = \frac{\sqrt{\pi}}{4}\left(2\langle A_0\rangle \frac{m\varepsilon_0}{e^2}\,\omega_p^2 v_t + \varepsilon_0 v_t E_{\mathrm{RF}}^2 \cdot \left(\frac{\omega_p}{\omega}\right)^2 \left(1 - \exp\left\{-\frac{\omega^2}{\omega_p^2}\right\}\right)\right). \tag{27}$$

Fig. 2 compares the averaging functions $G(\omega/\omega_p)$ and $(1-\exp\{-(\omega^2/\omega_p^2)\})$. Note that at high density levels (when f/f_p is small), the value of the averaging function, for the case in which shielding is taken into account, is about a factor of 2 higher than for the case in which space charge effects are ignored, because a greater fraction of particles has a flight time long enough to allow acceleration toward the limiting energy A_c. At high values of f/f_p, where the charge density is low, the averaging functions converge.

IV. Simulation Results

Let us first compare the above analytic theory with results obtained from the PIC-code XPDP1. Fig. 3 shows the impact energy spectrum. The predicted dropoff at $A_i = A_c$ is clearly apparent. Fig. 4 shows how the potential varies with distance. The discrepancy between the theoretical estimate for the potential, and of the potential realized in the code, is caused by electrons escaping across the diode, thus leading to imperfect shielding of the electric field. Fig. 5 shows how the average impact energy varies with RF field strength, exhibiting the predicted square law dependence [cf. (21)]. Fig. 6 shows impact energy again, concentrating on the averaging function, $G(\omega/\omega_p)$ of (21), as the injection current (recall that $J_0 \propto \omega_p^2$) is varied,

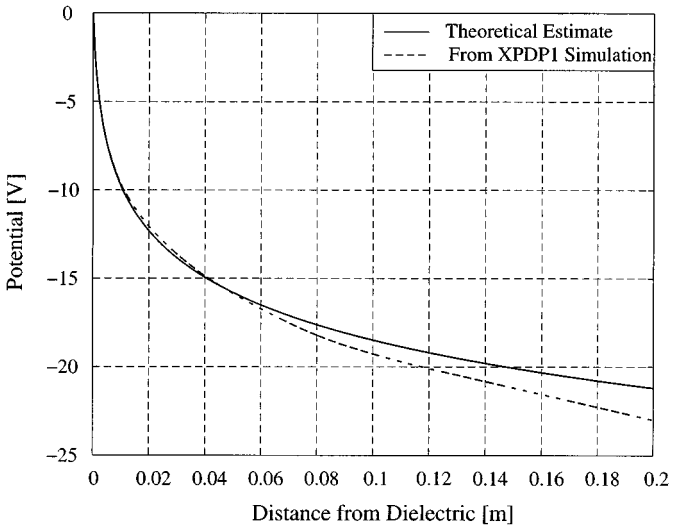

Fig. 4. Potential calculated for standard parameters.

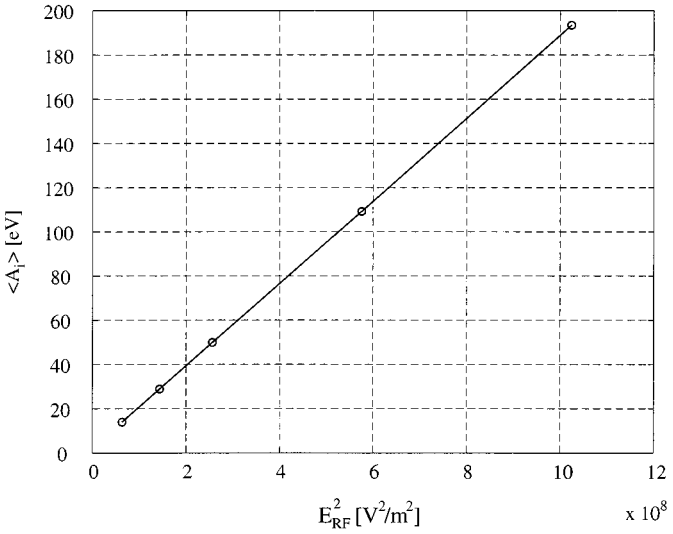

Fig. 5. Variation of average impact energy with RF field strength. Circles denote results from XPDP1, and the solid line is a curve fit.

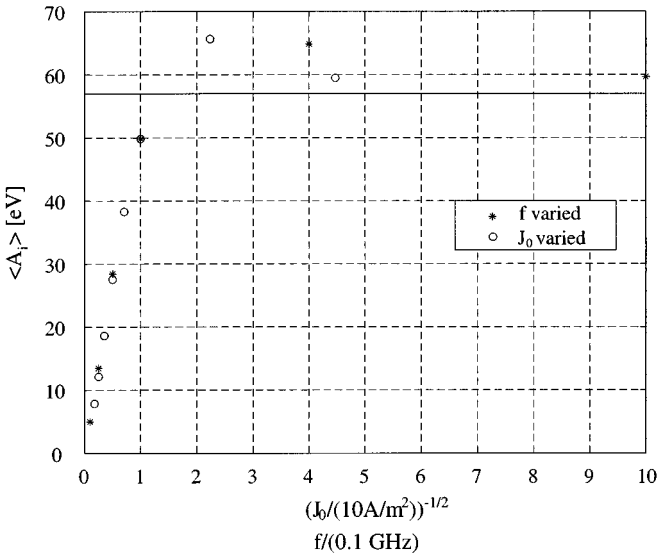

Fig. 6. Effect of the averaging function. Alternate variation of injection current density and RF frequency. Note that when the frequency is varied, the RF field strength is also varied to keep the ratio E_{RF}/f constant at a value of 1.6×10^{-4} [Vs/m]. The horizontal line depicts the maximum average energy gain according to (5), and it is equal to one-fourth of the value of the dropoff energy, A_c, according to (29).

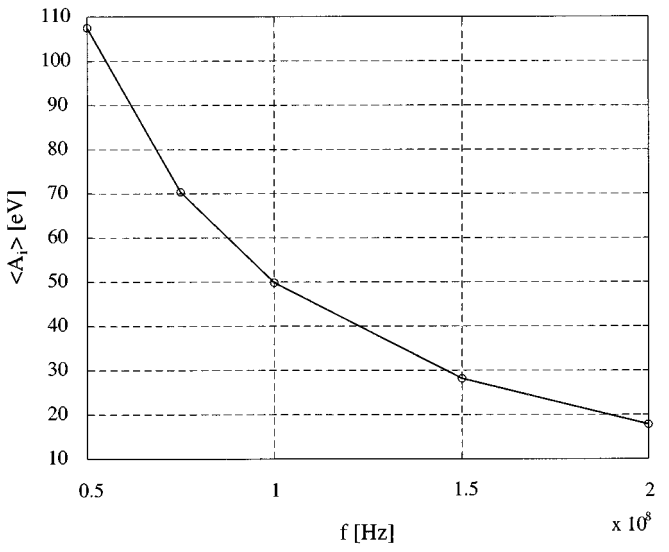

Fig. 7. Variation of average impact energy with RF frequency. Circles denote results from XPDP1, and the solid line is a curve fit.

and as the frequency is varied while keeping the ratio E_{RF}/ω constant (compare Figs. 2 and 6). The expected saturation level is fairly well met; however, it is exceeded at two points, but that is most likely a statistical or numerical effect. Fig. 7 shows the effect of varying the RF frequency, keeping other parameters constant. The average energy scales like $1/f$ in this region as $G(\omega/\omega_p)$ scales in a roughly linear fashion in this parameter range (see Fig. 6). For higher values of f, where the G-function levels off, we may expect the average energy to scale like $1/f^2$.

The comparisons with the PIC-code are favorable and seem to validate the analysis. The most interesting question is now to be answered, namely, what are the values of key parameters, such as the electron density and power delivered to the dielectric at saturation? To answer this question, we use a Monte-Carlo code to generate electrons emitted normally from the dielectric with a Maxwellian distribution in velocity, as described by (10), and a uniform distribution in the RF phase, θ. Using the equations we have for the flight time and energy gain, we may calculate their impact energy, whereas the impact angle, ξ, is found to be (see Fig. 1)

$$\xi = \tan^{-1}\left(\frac{eE_{\mathrm{RF}}}{m\omega v_0}(\cos\{\omega\tau+\theta\}-\cos\theta)\right). \qquad (28)$$

Then, given the impact energy and impact angle, (1) may be used to calculate a secondary emission yield for that particular electron. If we assume a thermal velocity, for a given RF field (magnitude and frequency specified), the only free parameter is ω_p, which corresponds to the secondary electron flux. The plasma density may then be set, so that the average secondary emission yields equal unity, corresponding to the steady state. As soon as the steady-state plasma density is found, our analytic

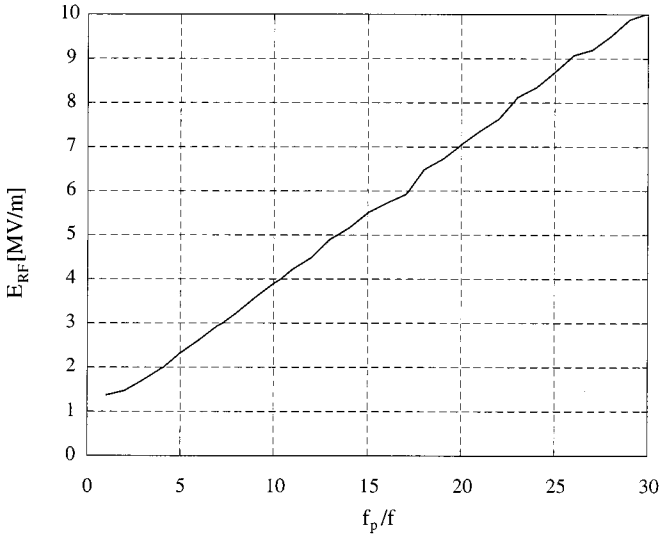

Fig. 8. Saturation curve for $A_{\max 0} = 420$ eV, $\delta_{\max 0} = 3$, and $kT/e = 2.8$ eV.

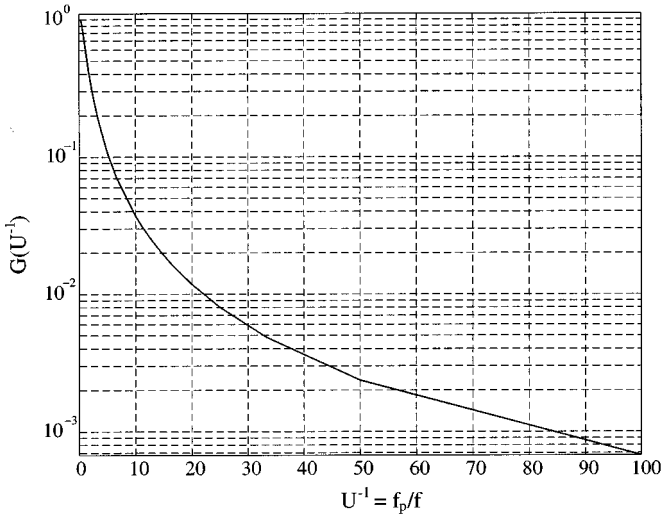

Fig. 9. Alternate diagram of averaging function, $G(U^{-1})$, for shielded case.

theory then yields the energy spectrum, average energy, density profile, power deposited to the dielectric, etc.

Using the Monte-Carlo approach, it is a simple matter to construct a curve, relating the parameters $E_{\rm RF}$ and ω/ω_p (or, equivalently, f/f_p). Fig. 8 shows such a curve. Given the magnitude and frequency of the RF, we readily read the value of f_p from the graph. Having determined the plasma frequency, we may turn to Fig. 2, or the equivalent Fig. 9, to determine the value of the averaging function. Using (21), we may calculate the average energy of electrons hitting the surface

$$\langle A_i \rangle = \langle A_0 \rangle + \frac{A_c}{4} G\left(\frac{f}{f_p}\right) \tag{29}$$

with A_c given in (6). Then, we may proceed directly to obtain the incident power density, by rewriting (24) in the useful form

$$P[\mathrm{W/m^2}] = 1045\sqrt{\langle A_0[\mathrm{eV}]\rangle}\,(f_p[\mathrm{GHz}])^2\langle A_i[\mathrm{eV}].\rangle \tag{30}$$

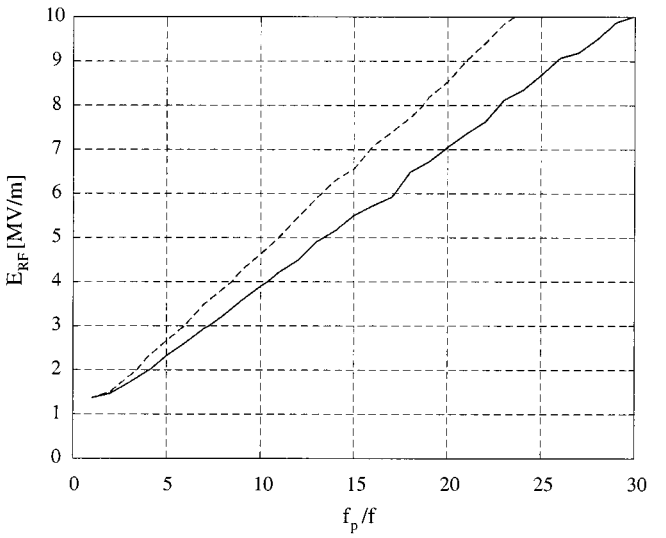

Fig. 10. Comparison of saturation curves for $A_{\max 0} = 420$ eV, $\delta_{\max 0} = 3$, and $kT/e = 2.8$ eV, with shielding effects (solid line), and without shielding effects (dashed line).

TABLE I
ILLUSTRATION OF IMPORTANCE OF SHIELDING, $A_{\max 0} = 420$ eV, $\delta_{\max 0} = 3$, $kT/e = 2.8$ eV, $E_{\rm RF} = 3$ MV/m, AND $f = 2.85$ GHz

	Shielding Included	Shielding Excluded
J_0 [MA/m^2]	1.15	0.696
$\langle\delta\rangle$	0.999	1.019
f_p/f	9	7
$\langle A_i \rangle$ [eV]	113	53
max(A_i) [eV]	9132	1218
P [MW/m^2]	130	37

To illustrate the effect of the shielding by space charge, Fig. 10 depicts saturation curves with and without space charge effects, for comparison. Note that higher charge density is reached at saturation when space charge effects are included.

The results of a sample calculation, comparing results obtained with and without shielding, are shown in Table I. The following parameters are used for the calculation: $f = 2.85$ GHz; $E_{\rm RF} = 3$ MV/m; $A_{\max 0} = 420$ eV; $\delta_{\max 0} = 3$; and $v_t = 9.92 \times 10^5$ m/s, i.e., $kT/e = 2.8$ eV.

When shielding is ignored, we arrive at the result (for $f/f_p \ll 1$, which is the most common case) that $P \propto E_{\rm RF}^2$, namely, that the power deposited is a fixed fraction of the incoming RF power (usually on the order of 1%). This is not necessarily the case when shielding effects are included.

V. CONCLUDING REMARKS

A few questions arise in conjunction with the results we have obtained so far. First of all, we note that the electron density at the surface is typically substantially higher than the critical density for the incoming RF. Now, we compare the length scale of the density v_t/ω_p, from (15), with the plasma skin depth c/ω_p and realize that the length scale is much smaller than is the skin

depth; hence, no appreciable decay of the RF will occur within the multipactor discharge.

Another question is whether loss of electrons from the discharge (in our model, they drift across the diode) will affect our results. If the characteristic length of the system is L, we find from (18) that the electrons that will be lost are those emitted with velocity v_0, such that

$$\left(\frac{v_0}{v_t}\right)^2 > 2\ln\left(1+\frac{\omega_p L}{v_t}\right). \tag{32}$$

The limiting number given by the right-hand side of (32) is typically greater than five, so that a small fraction of the emitted electrons (less than 1%) will be lost. Hence, the potential is not greatly altered. Then, we wonder how the average impact energy is affected, because those electrons with the longest flight time now add no energy to the surface. Simulations reveal that the average energy is in fact not affected, to any extent, by the loss of these electrons. This process can be understood by realizing that the majority of those particles, whose impact energy approaches the upper limit A_c, are not lost from the discharge.

A third consideration is the effect of the RF magnetic field. Because the magnetic force on the particles is proportional to their velocity, we may expect the magnetic field to affect only the higher energy electrons. Simulations using XPDP1 show that for relatively low values of the maximum attainable energy, $A_c < 1$ keV, the energy spectrum is identical despite whether an RF magnetic field is included. Previous work on susceptibility to multipactor discharge [10] has shown that in the absence of space charge effects, a strong electromagnetic wave incident on the breakdown side of a dielectric the high-energy $(>1\ \text{keV})$ multipactoring electrons are pushed toward the surface by the magnetic forces. This process leads to saturation in the possible energy gain of the multipactoring electrons, which has been verified by simulation for test particles with RF electric field strengths ranging from 1 MV/m to 1 GV/m. More importantly, it should also be noted that in the steady state, most of the multipactoring electrons are low energy and, thus, not affected by the RF magnetic field. Hence, the effects of the RF magnetic field will not greatly alter the results of the analysis presented in this paper. Further study on magnetic field effects is desirable for completeness, however.

It should also be noted that, in general, the distribution function of emission velocities of the secondary electrons is not Maxwellian. The true distribution is more complicated. However, the Maxwellian approximation is adequate in terms of results, and it has the advantage that it yields a closed-form solution for the potential, which is very useful in illuminating the physics involved. The authors have also used a uniform distribution function in their analysis yielding similar results.

An important assumption made in our model is that the RF electric field is parallel to the surface of the emitter. Previous work [10] has shown that if the RF electric field has an angle of obliqueness of as little as 5° to the surface of the dielectric, it can have a great effect on the susceptibility to multipactor, as the RF now has a component that affects the flight time of the emitted electrons. It is likely that an oblique RF field may also be important with regard to saturation of the discharge. This issue needs to be further investigated.

It should also be noted that in a realistic multipactor discharge, the emission current density will vary with a frequency equal to the RF frequency, because the secondary emission is time dependent from the time variation of the RF field. We believe that our model correctly portrays the time-averaged physics of the system. This needs to be confirmed by use of a dynamic model, in which the emission current is calculated in a self-consistent manner, given the angle of incidence and impact energy of each incident particle.

Finally, let us summarize the main results of our work, as follows.

1) Shielding of the surface electric field is important with regard to the saturation of multipactor discharge quantitatively. The electron density in the discharge, at saturation, is higher than was expected when shielding effects were ignored. The power deposited on the dielectric is higher than was previously expected (typically, four times higher, i.e., both the impact energy and current are about a factor of 2 higher).
2) The energy spectrum of incident electrons has a cutoff at a prescribed value, Ac, given by (6). This is a maximum value; the RF magnetic field may actually limit the impact energy to a lower value.
3) A simple method of obtaining the power deposited on the dielectric by the multipactoring electrons is given by use of (30) and Figs. 8 and 9. Note that Fig. 8 is only applicable to certain material; i.e., it assumes fixed values of $A_{\max 0}$, $\delta_{\max 0}$, v_t, and k_s.
4) High-energy electron impact is enhanced because of space charge shielding, corroborating experiments made at Texas Tech University [9].

REFERENCES

[1] D. H. Priest and R. C. Talcott, "On the heating of output windows of microwave tubes by electron bombardment," *IRE Trans. Electron Devices*, vol. 8, p. 243, 1961.

[2] J. R. M. Vaughan, "Some high power window failures," *IEEE Trans. Electron Devices*, vol. 8, p. 302, 1961.

[3] S. Yamaguchi, Y. Saito, S. Anami, and S. Michizono, "Trajectory simulation of multipactoring electrons in an S-band pillbox rf window," *IEEE Trans. Nucl. Sci.*, vol. 39, p. 278, 1992.

[4] R. A. Rimmer, "High power microwave window failures," Ph.D. dissertation, University of Lancaster, U.K., 1988.

[5] R. A. Kishek, Y. Y. Lau, L. K. Ang, A. Valfells, and R. M. Gilgenbach, "Multipactor discharge on metals and dielectrics: Historical review and recent theories," *Phys. Plasmas*, vol. 5, p. 2120, 1998.

[6] R. A. Kishek and Y. Y. Lau, "Multipactor discharge on a dielectric," *Phys. Rev. Lett.*, vol. 80, p. 193, 1998.

[7] L. K. Ang, Y. Y. Lau, R. A. Kishek, and R. M. Gilgenbach, "Power deposited on a dielectric by multipactor," *IEEE Trans. Plasma Sci.*, vol. 26, p. 290, 1998.

[8] A. Neuber, J. Dickens, D. Hemmert, H. Krompholz, L. L. Hatfield, and M. Kristiansen, "Window breakdown caused by high-power microwaves," *IEEE Trans. Plasma Sci.*, vol. 26, p. 296, 1998.

[9] A. Neuber, D. Hemmert, H. Krompholz, L. L. Hatfield, and M. Kristiansen, "Initiation of high power microwave dielectric breakdown," *J. Appl. Phys.*, vol. 86, p. 1724, 1999.

[10] A. Valfells, L. K. Ang, Y. Y. Lau, and R. M. Gilgenbach, "Effects of an external magnetic field, and of oblique radiofrequency electric fields on multipactor discharge on a dielectric," *Phys. Plasmas*, vol. 7, p. 750, 2000.

[11] J. P. Verboncoeur, M. V. Alves, V. Vahedi, and C. Birdsall, "Simultaneous potential and circuit solution for 1D bounded plasma particle simulation codes," *J. Comp. Phys.*, vol. 104, p. 199, 1995.
[12] J. R. M. Vaughan, "A new formula for secondary-emission yield," *IEEE Trans. Electron Devices*, vol. ED-36, p. 1963, 1989.
[13] A. Shih and C. Hor, "Secondary-emission properties as a function of the electron incidence angle," *IEEE Trans. Electron Devices*, vol. ED-40, p. 1448, 1993.

Agust Valfells, photograph and biography not available at the time of publication.

John. P. Verboncoeur (M'94) received the B.S. degree with high honors in engineering science from the University of Florida, Gainesville, in 1986. He received the M.S and Ph.D. degrees in nuclear engineering from the University of California, Berkeley, in 1987 and 1992, respectively, where he was a recipient of the DoE-administered Magnetic Fusion Energy Technology Fellowship.

In 1992, he joined the Plasma Theory and Simulation Group (PTSG) in Electrical Engineering at the University of California at Berkeley, as a Postdoctoral Researcher, to lead a pioneering effort to apply object oriented techniques to plasma simulation codes. The resulting code, XOOPIC, remains the keystone of the Berkeley plasma simulation code suite. From 1994-1996, he also worked as a Postdoctoral Researcher at the Lawrence Livermore National Laboratory, Livermore, CA, applying particle-in-cell, fluid, and Boltzmann computational models to plasma display panels. Since 1996, he has worked as a Research Engineer and co-leader of the PTSG at the University of California at Berkeley. His research interests are in theoretical and computational plasma physics, defined broadly to include electromagnetics, vacuum electronics, beam optics, plasma discharges, and numerical methods and algorithms. He is author or co-author of the Berkeley suite of particle-in-cell Monte Carlo collision (PIC-MCC) codes, including XPDP1 and XOOPIC. He has authored or co-authored over 25 journal articles and book chapters, and has taught numerous workshops and minicourses on simulation. He has also worked on a number of projects outside academia, including the Strategic Air Command Executive Support System, the U.S. Postal Service Mail Forwarding System, and the TRW Credit Data Consumer Report System, in addition to developing and licensing a number of commercial software tools.

Y. Y. Lau (M'98), was born in Hong Kong, in 1947. He received the S.B., S.M., and Ph.D. degrees in electrical engineering from the Massachusetts Institute of Technology in 1968, 1970, and 1973, respectively.

He was an Instructor and, later, an Assistant Professor in Applied Mathematics at MIT from 1973 to 1979. He was with Science Applications Incorporation from 1980–1983, and with the Naval Research Laboratory from 1983–1992, both as a Research Physicist. Since 1992, he joined the University of Michigan at Ann Arbor as a Professor in the Department of Nuclear Engineering and Radiological Sciences, and in the Applied Physics Program. He has worked mostly on electron beams (negative mass, hose, and beam breakup instabilities, beam quality, two-beam accelerators), coherent radiation source (gyro-TWT, gyromagnetron, relativistic klystron, crossed-field sheath, noise and intermodulation), plasmas and discharges (vacuum arc, laser ablation, multipactor). He has 7 patents and more than 100 refereed publications. While at NRL, he won several Invention Awards and Publication Awards, and was the recipient of the 1989 Sigma-Xi Scientific Society Applied Science Award. He was elected Fellow of the American Physical Society in 1986, and was the recipient of the 1999 IEEE Plasma Science and Applications Award. He was a Guest Editor of the IEEE TRANSACTION ON PLASMA SCIENCE, Special Issue on High Power Microwave Generation (June, 1998). He currently serves as an Associate Editor of the Physics of Plasmas.